Miscibility gap in fluid dimyristoylphosphatidylcholine:cholesterol as ''seen'' by x rays

Frank Richter,[1,2,*] Gert Rapp,[3,†] and Leonard Finegold[4,‡]
[1]*European Molecular Biology Laboratory at DESY, Notkestraße 85, D-22603 Hamburg, Germany*
[2]*Department of Physics, E22 Biophysics, TU Munich, D-85748 Garching, Germany*
[3]*MPI for Colloid and Interface Sciences, c/o HASYLAB, DESY, Notkestraße 85, D-22603 Hamburg, Germany*
[4]*Department of Physics, Drexel University, Philadelphia, Pennsylvania 19104*
(Received 21 May 2000; revised manuscript received 12 December 2000; published 26 April 2001)

A binary mixture of dimyristoylphosphatidylcholine (DMPC) and cholesterol displays a fluid miscibility gap under excess water conditions. Effects due to the imperfect miscibility of the two amphiphiles are studied near to and far from thermodynamic equilibrium by time-resolved small angle x-ray diffraction. The experiment discloses that this mixture phase separates when leaving the miscibility gap upon heating, a transition that is not included in current phase diagrams. This transition appears to be reversible and shows a temperature hysteresis of only a few degrees. We suggest a model in which the transition is driven with increasing temperature by a movement of the cholesterol away from the hydrophilic-hydrophobic interface toward the hydrophobic core of the bilayer.

DOI: 10.1103/PhysRevE.63.051914 PACS number(s): 87.16.Dg, 61.10.Eq, 64.75.+g

I. INTRODUCTION

Our theme is to model the membrane of any eucaryotic cell by studying the following aspects of a typical long-chain lipid mixed with a sterol: (1) the phase instability known as the fluid-fluid immiscibility gap (Fig. 1). (2) the behavior of the cholesterol-rich and depleted domains in this gap and (3) the dynamics of the system as probed by millisecond temperature jumps. The membrane can be pictured as a sheet, composed primarily of (very approximately) cylinders of lipids and sterols, which have their axes normal (vertical) to the sheet; the sheet is double to form a bilayer, with the outsides (the exterior and interior of the cell) in an aqueous environment. (We omit proteins and other moieties here.) We use the popular experimental model of liposomes where the bilayers, in water, are stacked to provide a periodic lattice, that diffract x rays to yield a series of Bragg-like reflections.

An understanding of the structural properties of lipid mixtures is a first step toward understanding biological membranes. Among the hundreds of different lipids found in a cell membrane, only a few make up the great majority. Even a two-lipid system shows properties which neither of the two species possesses alone, owing to the limited compatibility of the two lipids. The two major sources of incompatibility—and hence immiscibility—are the differing molecular structures and a differing symmetry of their liquid crystalline phases.

Of particular interest from a biological viewpoint are fluid-fluid immiscibilities. These are expected to occur in binary mixtures with large structural differences, and when one component can form tilted phases [1]. The binary system studied here, dimyristoylphosphatidylcholine (DMPC) and cholesterol [2], displays the fluid-fluid miscibility gap [1,3,4] in a range of temperature and cholesterol concentration that is characteristic of cell membranes. In this mixture both reasons for incompatibility—different molecular structure and liquid crystalline phase—are present.

Due to its biological relevance [5]—cholesterol is an essential sterol for mammalian membranes [6]—the mixture of cholesterol in a saturated long-chain phospholipid has become a classical study case targeted with a variety of methods. A phase diagram (Fig. 1) based on small angle neutron scattering (SANS), electron spin resonance spectroscopy (ESR), differential scanning calorimetry (DSC), and theoretical modeling has been established [1]. Whereas the solid-solid and liquid-solid miscibility gaps are better understood, an indication of improper mixing in the fluid phase is derived from an increased thermal expansion coefficient [7] and lateral diffusion measurements [8].

The low temperature boundary of the fluid gap region is given by the main transition zone of DMPC:cholesterol, which is a first order phase transition. It has been shown that more than 10-mol % cholesterol widens the main transition, suppresses the ripple phase and changes the thermal behavior of the lamellar lattice spacing $d(T)$ of DMPC membranes [9]. Referring to the phase diagram (Fig. 1), the high temperature boundary separates the fluid-fluid miscibility gap from perfect miscibility. At the high temperature apex of the gap, equilibrium thermodynamics demands a hidden critical point to terminate the gap [1]. Monolayer studies provided the first experimental indication of the critical point [10]. That the mixture is expected to exhibit critical behavior is of particular interest, because the accompanying long range fluctuations in concentration may affect enzyme activity or may mediate a long range protein-protein interaction [11]. However, recent NMR studies over the gap region [12] showed no modification of the average orientation of cholesterol, and a monotonic decrease of the molecular order parameter S_{mol} with temperature.

Physically, the molecular arrangement in the binary mixture DMPC:cholesterol is pictured by numerical simulations

*Electronic address: efrichter@web.de
†Electronic address: gert.rapp@desy.de
‡Electronic address: L@drexel.edu

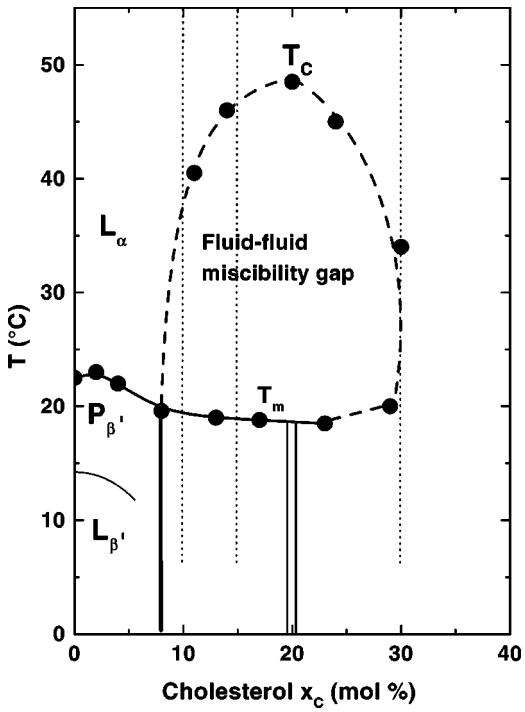

FIG. 1. Partial phase diagram of the binary mixture DMPC:cholesterol, showing the location of the fluid-fluid miscibility gap (adapted from Sackmann, 1995 [1]; circles refer to data for the phase boundaries as obtained from DSC, ESR, and SANS). T_m denotes the main transition temperature. Note that only the bottom boundary of the fluid-fluid miscibility gap, i.e., the main transition, is experimentally well documented. The bold faced line at 8 mol % marks the continuation of the fluid miscibility gap into the gel phase, and also indicates the maximum cholesterol concentration miscible. Cholesterol concentrations up to this level thus do not alter the phase sequence, with temperature, of the lipid. The two parallel lines centered about 20-mol % cholesterol indicate the stoichiometric 4:1 mixture; note that the 4:1 mixture is in the vicinity of the ''hidden,'' and thus metastable, critical point T_c at the top of the fluid gap. A sample, positioned in the phase space extending to higher temperatures than the upper boundary, is presumed to be in the miscible state. The dotted lines represent the temperature scans run, and used, in this work.

such as the occurrence of cholesterol-rich and cholesterol-depleted domains, sometimes called l_o and l_d [13,14]. Their sizes are determined by the balance of the chemical and the elastic interfacial energies, resulting in a two-dimensional pattern formation. The basis of this immiscibility picture of the lipid-cholesterol mixtures is a two-dimensional (2D) surface, i.e., the segregation is lateral [15]. The two types of domains are expected, due to their different chemical composition, to have differing lattice spacings. Therefore, x-ray scattering appears to be a suitable tool to explore the fluid-fluid miscibility gap.

II. EXPERIMENT

A. Protocol

Lipids and cholesterol were used as purchased from Avanti (Alabaster, AL) and androsten (androsten-3β-ol) from Steraloids (Wilton, NH). Aqueous suspensions of multilamellar vesicles (25 wt.% lipid content) were prepared in bidistilled water [9,16], filled into x-ray capillaries and flame sealed. Samples containing 0-, 10-, 15-, and 30-mol % cholesterol ($x_c = 0.00$, 0.10, 0.15, and 0.30) were used.

To study structural changes while changing temperature, we conducted time-resolved small angle x-ray diffraction experiments at beam line X13 of the European Molecular Biology Laboratory (EMBL) at Deutsches Elektronen-Synchrotron (DESY) [17]. All samples were heated from 10 to 70 °C, and subsequently cooled back to 10 °C at a rate of 1 K/min, with exposures of 5 s taken twice a minute. For the laser-induced temperature jumps [17,18] we chose base temperatures between 10 and 70 °C. A jump amplitude of 20 °C within a 2-ms laser pulse was achieved. The structural response of the system to nonequilibrium conditions was monitored in a series of 100-ms exposures for each base temperature. At each base temperature the jump was repeated four times to investigate the reproducibility of the structural response. All data recorded were normalized to the incident intensity of the x-ray beam, and calibrated against dry Ag-behenate powder [19].

B. Data analysis

The state of matter of amphiphilic systems is that of liquid crystals. Thus they develop only quasi-long-range order, in contrast to the long-range order found in crystals. The quasi-periodic lattice seen by x-ray diffraction is disturbed by two types of disorder, i.e., defects of the first and second kinds. Whereas the first kind is of dynamic origin and reduces the maximum intensity of the reflections, the second kind is static, i.e., stacking defaults [20]. Static defects also broaden the line shape with increasing diffraction order. As a consequence of these types of defects, a significant portion of the scattered photons contributes to far reaching reflection tails.

The line shape of lipid membrane reflections has been modeled to theories for liquid crystals [21–23] to determine the membrane form factor, and hence to reveal the membrane structure. The fit parameters used are—among others—the size of the scattering domains and the elastic moduli. In time-resolved measurements we focus on structural changes induced by changing a thermodynamic variable such as the temperature T, the pressure p, or the chemical potential μ. The structural changes result in a line shape change. Compared to static $\vartheta - 2\vartheta$ scans, the time-resolved data contain a larger contribution due to instrumental broadening. Then any fit would not reveal the sample's properties. The sample's signal may be obtained by a deconvolution of the measured diffraction pattern by the instrument's transfer function; the quality of this depends on the spatial resolution of the detector system, the beam characteristics, and the signal-to-noise ratio (to achieve a high time resolution and a high resolution of the diffraction pattern are mutually conflicting goals).

To investigate the structural changes we determine the thermal behavior of the lattice spacing $d(T)$; the lamellar unit cell contains a bilayer and an adjacent interlamellar water layer,

$$\frac{1}{d}=\frac{\sum_{s_{min}}^{s_{max}}|s-s(I_{max})|I_s}{\sum_{s_{min}}^{s_{max}}I_s}, \tag{1}$$

where I_s is the intensity of a reflection at a scattering vector s. We thus consider a reflection as a statistical distribution of the photons scattered in the range $[s_{min},s_{max}]$. Then, $1/d$ is defined as the mean of this distribution. A discrete representation of a reflection is chosen because of the finite resolution of the detector system. At the summation boundaries s_{min} and s_{max}, the diffraction signal is indiscernible from the low noise level. The lower and upper boundaries are selected in such a way that a further extension of the summation interval does not change the value of $1/d$ for the broadest reflection measured; in this work, $(s_{max}\text{-}s_{min})=0.05\ \text{nm}^{-1}$.

The summation procedure does create a systematic error in the lattice spacing d when the tails beyond the summation limit are asymmetric [24]. Relative changes with temperature in d do not suffer from systematic errors as long as the asymmetry of the tails beyond summation limits does not change. The main error contribution arises from the error Δs in s, as given by the spatial resolution of the x-ray camera-detector setup. In this experiment $\Delta s=0.000\,276(3)\ \text{nm}^{-1}$. The overall experimental error is obtained by adding the mean square root errors. Where two or more reflections overlap over the course of the experiment, the summation range to determine the lattice spacing d of one of the two reflections is purposely limited to the distance defined by the maximum position $s(I_{max})$ and s at the minimum between the two overlapping reflections.

III. RESULTS

A. Data

Figure 2 shows the sequence of diffraction patterns recorded from a DMPC mixture with $x_c=0.15$ during a heating and cooling cycle. According to the phase diagram (Fig. 1) a sample with $x_c=0.15$ enters the miscibility gap at about 19 °C and exits at about 48 °C. A visual inspection of the diffraction scan (Fig. 2) shows a strong nonlinear decrease in the intensity of both diffraction orders with increasing temperature, over the temperature range of the fluid miscibility gap and beyond. We found the same behavior in similar experiments (unpublished data from this lab) with dipalmitoylphosphatidylcholine (DPPC) and cholesterol ($x_c=0.00$, 0.10, 0.15, and 0.30), and with DMPC and androsten (the same sterol concentrations).

At higher temperatures the reflections are split, as can be seen better at second order (Fig. 2). This splitting is in apparent contradiction to a perfect miscibility, as implied in the phase diagram (cf. Fig. 1). The same splitting is observed at temperatures above the range of the gap [Fig. 3(a)] in the DMPC:cholesterol mixtures, but not for the reference mixtures DPPC:cholesterol and DMPC:androsten.

A split of the single lamellar phase into two coexisting lamellar phases is evidence of a structural phase transition.

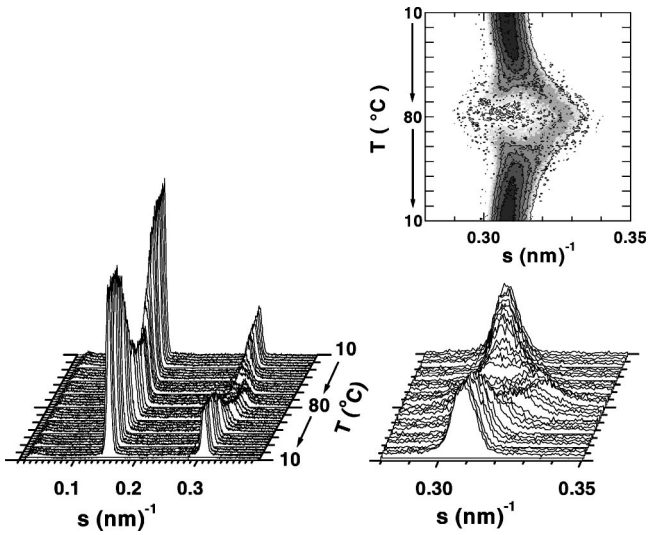

FIG. 2. X-ray diffraction patterns recorded on heating and cooling scans as a function of scattering vector s ($s=1/d=2\sin\vartheta/\lambda$, with 2ϑ the scattering angle) through the miscibility gap of a DMPC:15-mol % cholesterol sample. The bottom right plot magnifies the second order reflection. Top right: intensity contour plot of the second order reflection as a function of temperature T and scattering vector s. This representation highlights the splitting transition and its reversal.

The splitting transition appears to be reversible, and has a temperature hysteresis of only a few degrees (Fig. 3), comparable in size to the hysteresis of the main transition in one-component lipid systems in excess water. There the thermodynamic viewpoint links the narrow hysteresis to a high degree of cooperativity of the chain melting [25].

A phase separation was also observed in DMPC:cholesterol monolayers by fluorescence spectroscopy [26]. X-ray diffraction probes the long-range ordering along the bilayer normal, thus our data demonstrate that the phase separation we observe is not confined laterally in the plane of a bilayer.

B. Fluid-fluid miscibility gap

1. Behavior of the lattice spacing d

The temperature dependence of the lattice parameter $d(T)$ strongly depends on the cholesterol concentration x_c [Fig. 3(a)]. As long as the concentration is low enough, i.e., $x_c \leqslant 0.10$, the binary mixture has similar thermal behavior to the pure phospholipid [Fig. 3(a)], which suggests perfect miscibility. In the temperature range of the splitting regime ($T>45$ °C) the behavior of the of pure DMPC lattice is well described by a thermal expansion coefficient $\alpha=0.0092(1)$ nm/K.

The immiscibility of concentrations $x_c \geqslant 0.15$ results in a functionally different behavior of $d(T)$, as shown by the complete suppression of the precritical lattice swelling above the main transition seen for $x_c \leqslant 0.10$ [9]. Also, the lattice parameter $d(T)$ for $x_c \geqslant 0.15$ does not show a thermal hysteresis. In particular, over the region of the miscibility gap—roughly 20–50 °C, 10–30-mol % cholesterol (Fig. 1)—the lattice spacings only very gently decrease with temperature

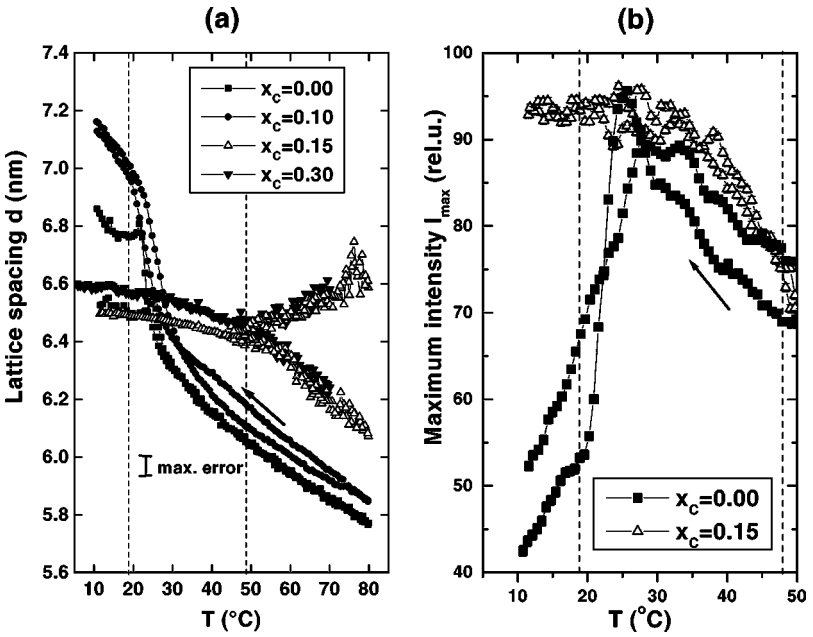

FIG. 3. (a) Lattice spacing d and (b) maximum intensity I_{max} (in relative units) of the first order reflection as functions of temperature T observed in the diffraction scans of DMPC:cholesterol mixtures. In both panels, symbols denote the same cholesterol concentration. Data recorded on heating and cooling for each sample are shown. An arrow indicates the scan direction, and hence a hysteresis between heating and cooling. The hysteresis in the d spacing of the $x_c=0.10$ sample could be related to its vicinity to the miscibility-immiscibility border. The dotted lines approximately mark the extreme boundaries of the fluid miscibility gap, according to Fig. 1. The maximum error bar shown in (a) results from the weak intensity of the split reflections at high temperatures; for the nonsplit reflections the error is of symbol size.

[Fig. 3(a)] before undergoing the splitting transition. Then an analysis of the thermal behavior of the d spacing may be used to distinguish between fluid miscibility and immiscibility in our system [Fig. 3(a)].

Above the gap the short lamellar spacing shows a similar temperature dependence to that of the pure DMPC, whereas the long lamellar lattice slightly expands with temperature [Fig. 3(a)]. Figure 4 displays the difference $\Delta d = d_{short} - d_{DMPC}$. Δd obtained from the samples showing the splitting remains in a range of [0.3,0.45] nm, with a tendency to decrease at higher temperatures.

2. Behavior of the maximum intensity I_{max}

With increasing temperature the maximum intensity of the reflections decreases [Figs. 2 and 3(b)]. The intensity decrease for $x_c=0.15$ over the range of the gap is quantitatively not different from that of DMPC, in contrast to the changes in their lattice spacings [Fig. 3(a)]. The decrease may be fitted to the Debye-Waller form [20], that gives the maximum intensity I_{max} as function of the scattering vector s,

$$I_{max}(n) = I_0 \exp(-4\pi\langle\mu^2\rangle s_n^2), \tag{2}$$

with I_0 the intensity for a static lattice ($T=0$), $\langle\mu^2\rangle$ the mean square displacement of the membranes and s_n the scattering vector of nth diffraction order. Having measured the maximum intensity $I_{max}(T)$ and the scattering vector $s(T)$ of a reflection, we may obtain the mean square fluctuations $\langle\mu^2\rangle(T)$ (Fig. 5). Clearly, our $\langle\mu^2\rangle$ data are large considering the lamellar unit cell size of about 6 nm, indicating that our $\langle\mu^2\rangle$ analysis may not give quantitatively correct data for the mean square fluctuations of the lamellar lattice. Though we may question the applicability of Eq. (2) to lipid membranes, we note that $\langle\mu^2\rangle$ seems to distinguish between samples inside and outside the gap, as the data for $\langle\mu^2\rangle$ from the mixtures in the gap are significantly larger (Fig. 5). Further, $\langle\mu^2\rangle$ does not change until the system undergoes a phase transition: the macroscopic splitting into the small and long lamellar spacings for samples in the gap, and the main transition (including the swelling regime) for samples outside the gap [Fig. 3(a)]. Technically, the differences in $\langle\mu^2\rangle$ here are due to the different temperature dependence of the lamellar lattice spacing and not to differences in the maximum intensity (cf. Fig. 3). Also, the difference in the maximum intensity I_{max} between heating and cooling for the low-x_c mixtures [Fig. 3(b)] leads to a hysteresis in $\langle\mu^2\rangle$. The temperature hysteresis of the lattice spacing d for $x_c=0.10$ [Fig. 3(a)] results in a changing $\langle\mu^2\rangle$ on cooling. Whereas the power to distinguish between miscible and immiscible samples of the thermal behavior of the lattice spacing d [cf. Fig. 3(a)] may be a secondary effect caused by the mixture's swelling behavior [9], the $\langle\mu^2\rangle$ analysis appears to be ca-

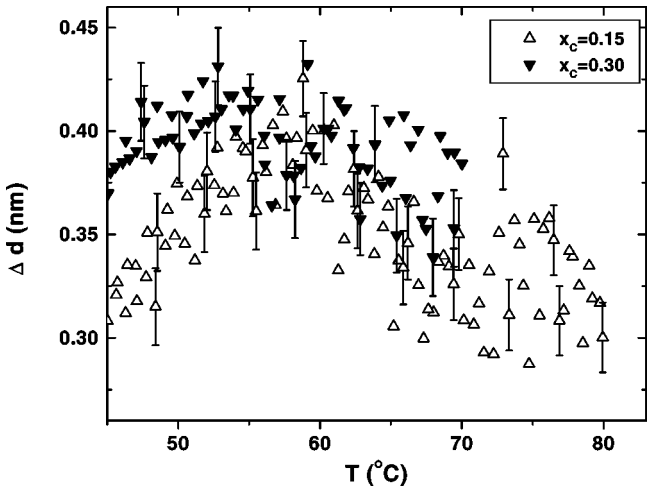

FIG. 4. Difference in the lattice spacing Δd between the short lamellar and the pure DMPC: All data where the splitting is observed are included, i.e., from heating and cooling of the samples $x_c \geqslant 0.15$. Except for the low temperature end adjacent to the miscibility gap (where the overlap of the two split reflections is significant), the data for both samples agree within experimental error.

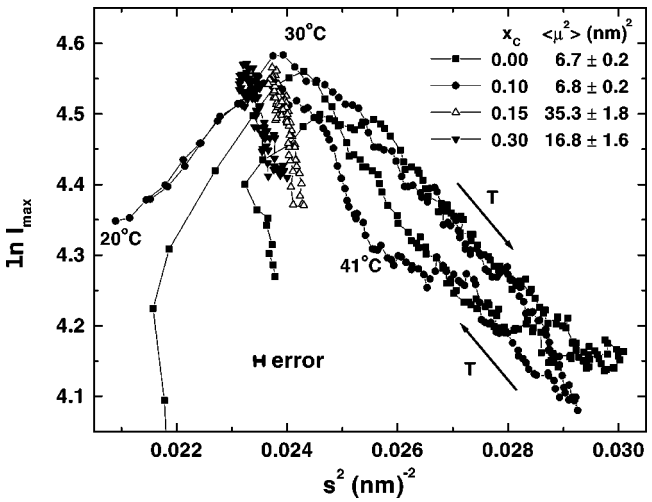

FIG. 5. Logarithm of the maximum intensity I_{max} of the first order reflection as function of the square of the respective scattering vector s. The symbol code is as in Fig. 3. For $x_c=0.00$ and 0.10, the data shown refer to a heating-cooling cycle (indicated by arrows) over the range of 20–80 °C; for $x_c=0.15$ and 0.30 only data collected in the range of the miscibility gap (20–45 °C) are considered. The data given for $\langle\mu^2\rangle(T)$ were fitted over the heating range of 33–72 °C for $x_c=0.00$ and 0.10, and 30–45 °C for the other two concentrations. These ranges are the most extended over which the samples display an approximately constant $\langle\mu^2\rangle$. A few data points at $x_c=0.10$ have been temperature labeled. The positive slope for samples $x_c\leqslant 0.10$ and low s^2 is related to the main transition. The error in s^2 is roughly the same for all samples, as all scans were measured using the same x-ray camera settings. Errors in the logarithmic intensity are well within symbol size.

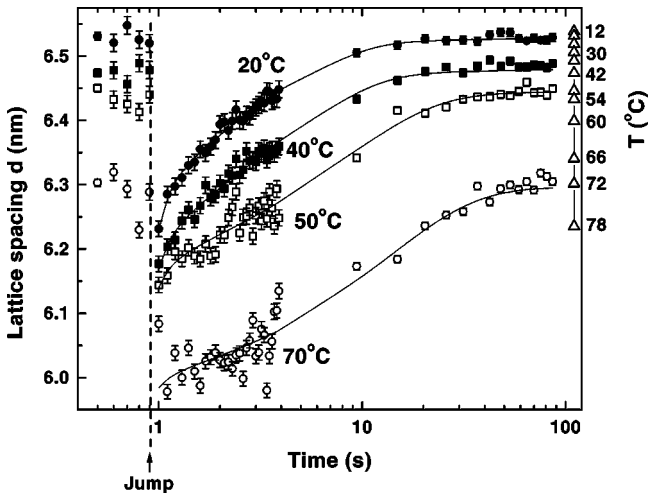

FIG. 6. Structural response to laser-induced nonequilibrium conditions: The sample ($x_c=0.15$) reacts to the laser flash with a sudden decrease of the lattice spacing. For readability, only data for the four base temperatures (as indicated on the graphs) are shown; graphs of the other base temperatures interpolate. Full (open) symbols indicate a base temperature within (above) the miscibility gap. The up triangles to the right give the lattice spacings obtained from the scan data collected on the same sample ($x_c=0.15$) [cf. Fig. 3(a)]; spacings are shown in steps of 6 °C at the temperature indicated. The data are fitted to a sum of an allometric function and an exponential function (see text). Data for temperatures in the splitting regime refer to the short lamellar phase. The fit parameter values are listed in Table II.

pable of separating the phase transitional phenomena from the primary miscibility effects.

Given that a line shape analysis of static x-ray data from the fluid crystalline phase of DPPC yields $(0.85\ \mathrm{nm})^2$ for the mean square fluctuations [23], lattice fluctuations appear to be a minor contributor to the $\langle\mu^2\rangle$ obtained here for DMPC [$6.7\pm0.2\ \mathrm{nm}^2$ (Fig. 5)]. Further, cholesterol concentrations in the gap stiffen the membrane [27].

C. Mixture under nonequilibrium conditions

Measurements away from equilibrium are well suited to study the nonequilibrium kinetics of a system. For this experiment the sample with $x_c=0.15$ was selected because of its positioning with respect to the gap. By heating with a laser pulse (heating rate 20 K/2 ms) we certainly drive the system out of thermodynamic equilibrium. Thus we may expect a different structural response to the strong perturbation compared to the near-equilibrium scan data presented above. Table I gives the recording protocol of the temperature jump experiment. The structural parameter that can be determined the most accurately in highly time-resolved diffraction studies is the lattice spacing. To detect a reflection with a virtually noise-free gas detector requires only a few scattered photons [28]. Figure 6 shows the temporal evolution of the d spacing in response to the laser-induced nonequilibrium conditions for selected base temperatures.

TABLE I. Recording protocol for the laser-induced temperature jump experiment. The first frame (diffraction pattern) is used to determine the lattice spacing prior to a temperature jump. Frames 2–5 determine the signal-to-noise ratio, and thus set the upper limit for time resolution achievable for a particular sample. The following frames record the relaxation process. Comparison of the first and last frames can verify the reproducibility of the diffraction signal before and after the temperature jump. A wait time of 5 μs between two subsequent frames is the minimum required by hardware.

Frame	Wait time (ms)	Recording time (ms)	Total time (s)	Remarks
1	0.005	500	0.5	control
2–35	0.005	100	3.9	laser pulse after frame 5
36–50	5000.000	500	86.4	

TABLE II. Least-squares fit to the relaxation of the lattice parameter d by a sum of an allometric decay (mechanism A) and an exponential decay (mechanism B) as described in the text for base temperatures in the gap and in the splitting transition for the sample $x_c = 0.15$. The minus sign in τ_A originates from the fact that we model the difference to the safely measured equilibrium spacing d_0; we would obtain a positive exponent if we were to model the difference to the shortest spacing immediately after the jump. The accuracy with which this spacing is detected depends on the signal-to-noise ratio, and thus on the recording time of this first frame following the jump (here frame 6, cf. Table I), and on the duration and energy of the laser pulse which is deposited in the sample. The parentheses contain the least squares error resulting from the fit.

Base temperature (°C)	d_0 (nm)	d_A (nm)	τ_A	d_B (nm)	τ_B (s)
10	6.532(6)	0.009(10)	−0.90(50)	0.15(2)	2.3(0.2)
20	6.531(6)	0.037(07)	−0.57(06)	0.17(1)	3.1(0.2)
30	6.514(6)	0.045(08)	−0.51(05)	0.18(1)	4.1(0.4)
40	6.474(6)	0.030(03)	−0.48(08)	0.20(1)	3.8(0.2)
50	6.450(6)	0.037(13)	−0.40(11)	0.22(2)	8.5(1.4)
70	6.303(6)	0.030(10)	−0.30(05)	0.26(1)	13.3(2.0)

The main observations are the following: (1) For all base temperatures the sample's d spacing relaxes back to its size prior to the jump. (2) Moreover, this size equals the size determined during the slow scan (Fig. 6, right axis). (1) and (2) imply that the unit cell size within the multilamellar stack is always recovered. Recovery takes more time at higher temperatures.

The lattice spacing immediately measured after the jump for the lowest base temperature shown (20 °C) is equal to a near-equilibrium spacing at 78 °C (Fig. 6). A corresponding temperature jump amplitude of 58 °C is higher than the temperature rise due to the energy deposited by the laser pulse to lipids in water [18]. This means that the sample attains a nonequilibrium state. The change in the lattice spacing due to the jump is, for all base temperatures, about 0.3 nm, i.e., the characteristic size of a water molecule.

The relaxational behavior from nonequilibrium follows a time course dependent on the initial state (cf. Fig. 1). As long as the sample was, prior to the jump, in the miscibility gap [$T < 45$ °C, from Fig. 3(a)] the lattice parameter relaxes in a nonlinear, but not simply exponential, fashion (cf. Fig. 6 and Table II). At base temperatures above the splitting transition, the lattice spacing changes gradually over the first 1.5 s following the jump. The changing response to the nonequilibrium conditions is seen the best when comparing the experiments of base temperatures 20 and 70 °C (Fig. 6). We remark that a fluid membrane should maintain its lattice parameter for a few seconds after the jump, followed by an exponential increase due to the then effective passive cooling [18].

A double exponential decay has been used to fit the nonequilibrium response over the pretransition of DPPC [29]. The reduced lattice parameter d in response to the laser pulse should be either attributed to a change of the interlamellar water layer or a change of the DMPC:cholesterol bilayer. In particular, for higher base temperatures, we find the following two-process description fits better: the lattice expansion during passive cooling and a change of the interlamellar water due to diffusion are described by an exponential. The allometric term is motivated by the observation that, e.g., in alloys [30], the final growth of the domains follows a $t^{1/3}$ law [31] to describe the relaxation of the domain structure in the bilayer:

$$d(t) = d_0 - d_A t^{\tau_A} - d_B \exp(-t/\tau_B). \tag{3}$$

Here d_0 is the equilibrium spacing measured at the base temperature; d_A, d_B, τ_A, and τ_B denote the amplitudes and decay constants of the two relaxation processes A and B. The zero time for the fit is set after the laser flash ($t = 0.902$ s, cf. Table I). Table II summarizes the fit parameters: the data for d_B indicate that the diffusional relaxation process B contributes more at higher base temperatures. Further, process B slows down with increasing base temperature. The relaxation time of the diffusion τ_B roughly doubles while the base temperature is raised from 40 °C (within the gap) to 50 °C (in the splitting regime). Thus, the diffusional processes slow down under the macroscopic phase separation.

The amplitude of mechanism A, d_A, appears to be less sensitive on the base temperature, but the magnitude of the exponent decreases with increasing temperature. At the lowest base temperature of 10 °C, where the sample is in the solid miscibility gap, this process is only marginally relevant (Table II). Presumably the power law relaxation describes the response of the bilayer, we may compare this to a nucleation and growth scheme. We note that the magnitude of τ_A approaches the Lifshitz-Slyozov value of 1/3 with increasing base temperature. Then the (scaling) exponent τ_A characterizes the average domain size.

Over the first seconds following the temperature jump the diffusional mechanism is, for all base temperatures, the major contributor to the changes in the lattice spacing before mechanism A dominates [4 s (10 °C), 8 s (20 °C), 10 s (30 °C), 12 s (40 °C), 26 s (50 °C), and 44 s (70 °C)]. Table II shows that both decay constants depend on the initial state of the system.

The observed time dependence of the relaxational kinetics on the initial state—and not on the final state immediately after the jump—indicates that the degree of miscibility is conserved under nonequilibrium. Further, the decrease of the

lattice spacing during the jump is independent of the initial state. Since the laser energy is mainly absorbed by the water, this decrease is largely attributed to the structural units common to all phases observed: this commonality is the interlamellar water layer. This includes the water layer adjacent to the lipid bilayer.

IV. DISCUSSION

Our discussion aims to explain the unexpected phase transition observed at the upper bound of the miscibility gap by x-ray diffraction. The experiment reveals the following structural features: (1) The transition is completely reversed upon cooling [cf. Figs. 2 and 3(a)]. (2) Within the gap, DMPC and cholesterol form one lamellar phase, and above the gap they form two lamellar phases with different lattice parameters [Figs. 2 and 3(a)]. (3) The two lattices in the splitting regime show a different temperature dependence [Fig. 3(a)]. (4) The thermal behavior of the shorter-spaced lattice is similar to that of the DMPC lattice [Fig. 3(a)]. (5) The difference between the lattice spacing of the shorter-spaced lattice and the DMPC lattice varies within a small range (Fig. 4). (6) The response to nonequilibrium conditions in the splitting regime behaves similar to that of liquids (Fig. 6). (7) The relaxation is determined by the initial state (cf. Table II). (8) Analogous experiments on mixtures of DPPC-:cholesterol and DMPC:androsten do not show the splitting transition (unpublished data from this collaboration).

A. Domains as defects

In the splitting transition the domain structure of cholesterol-rich and cholesterol-depleted (micro)domains present in the gap (as supported by monolayer experiments [26]) macroscopically phase separates normal to the bilayer as we observe by x-ray diffraction. Primarily, the small domains within an individual bilayer are—in the light of x-ray diffraction—static defects, and reduce the long-range ordering. In the fluid-fluid gap region there is no domain formation normal to the bilayers [cf. Figs. 2 and 3(a)]. Nevertheless, the microdomains within the single bilayers may grow and coarsen laterally when approaching the upper temperature boundary of the miscibility gap, i.e., a demixing of lipid and cholesterol may proceed with increasing temperature. Reaching a characteristic size (in the splitting transition), the domain formation within individual bilayers becomes cooperative within the multilamellar stack. In this sense the fluid-fluid lipid:cholesterol mixture behaves in close analogy to a percolating system.

An ongoing demixing likely changes the membrane's dynamical behavior [32]. In addition, mechanical properties also depend on the cholesterol content [33], and so may affect the dynamical properties of the membrane [34].

Far-from-equilibrium conditions do not support a domain coarsening, which is a near-equilibrium phenomenon. The system does not, immediately after the jump, change from the demixed regime into a phase separated regime.

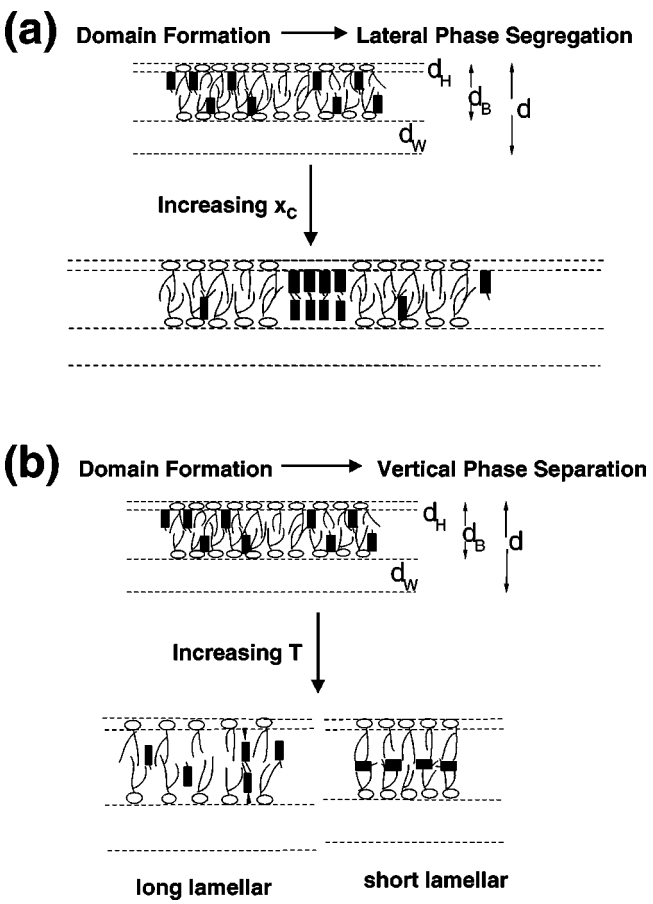

FIG. 7. Lateral vs normal movement of the cholesterol (dark symbols) in the lipid bilayer (open symbols): (a) Lateral movement leads to phase segregation, with cholesterol domains of limited size due to the hydrophobicity of cholesterol. (b) On the other hand, a vertical movement can lead to domains of macroscopic size extending along the bilayer normal. Here the cholesterol molecule orientation in the short lamellar phase is different from the other possibilities. (Note that a difference in the *d* spacing is pictured.) The lateral phase segregation (a) is triggered by an increasing concentration of cholesterol, which decreases the miscibility, while the vertical phase separation (b) is driven thermally.

B. Lateral vs vertical segregation

Here we introduce the possibility that cholesterol, as a mainly hydrophobic entity, can (a) not only move laterally but also normally (''vertically''), and (b) can reorientate parallel to the bilayer surface. A vertical movement is also supported by recent neutron scattering experiments [34]. Note that the interactions between a lipid and a cholesterol molecule are relatively weak [35]. Both movements (Fig. 7) could explain the splitting [Fig. 3(a)].

For a purely lateral phase segregation leading to a cholesterol-rich phase and a depleted phase, one could expect the depleted phase to reach a cholesterol concentration that is low enough for complete miscibility. Figure 3(a) shows that neither of the two split lamellar phases has a lattice spacing *d* close to that of the DMPC reference that is, by definition, perfectly miscible. Conversely, even the shorter spaced lattice maintains a clearly larger spacing than

that of DMPC with increasing temperature (cf. Figs. 3(a) and 4].

A presumed vertical movement of the cholesterol, the smaller *d* spacing and the larger *d* spacing are explained as follows [cf. Fig. 7(b)]: The long spacing may originate from domains in which the cholesterol has not changed its orientation with respect to the bilayer normal but has moved toward the center of the bilayer [34]. The slight increase in *d* with temperature is then caused by a reduced flexibility of the lipid chains. The thinner spacing could be obtained by the cholesterol changing its orientation perpendicular to the bilayer normal. Then the cholesterol is found in the center of the bilayer, and no more between the chains of one of the monolayers. A thin cholesterol layer at the bilayer center causes the methyl end groups of the two monolayers to interact with the cholesterol layer, replacing the direct interaction between the tails. We do not expect this change to be crucial for the thermal behavior as, e.g., the specific heat anomalies in lipid:cholesterol systems can be explained without invoking special lipid:cholesterol interactions [3,35]. The thermal contraction of the short lamellar lattice with rising temperature is then predicted to be similar to the pure DMPC [cf. Fig. 3(a)]. The thickness of the cholesterol layer can be estimated by subtracting the *d* spacing of the pure DMPC from the *d* spacing of the thin lamellar phase (cf. Fig. 4). The difference Δd compares well to the thickness of a single (anhydrous) cholesterol molecule (0.38 nm, estimated from crystallographic data [36]). The thin—compared to the unit cell size—and reoriented cholesterol layer also makes understandable the liquidlike, diffusion-dominated response to far-from-equilibrium conditions (cf. Fig. 6).

Given a vertical movement, the two observed lamellar phases differ primarily in their cholesterol orientation, and not in their cholesterol concentration. This effect is closely related to the nonspherical molecular architecture of both the molecule species. The very small temperature hysteresis of the completely reversed phase separation transition supports the vertical movement. The driving force could very well come from the hydrophobic-hydrophilic interface that changes with temperature. Once the cholesterol-rich domains have laterally grown to such an extent that it is energetically too costly to have large areas of high cholesterol density at the lipid-water interface, the cholesterol will tend to move toward the hydrophobic core until it becomes too costly to drag the hydroxy group further into the bilayer. The 2D picture of a solely lateral phase segregation appears to be better suited for an amphiphilic mixture such as DMPC:DSPC [37], as the interface does not change under a lateral demixing. Our 3D picture is based on the large difference in amphiphilicity of DMPC and cholesterol.

We supplement the phase diagram (compare Figs. 1 and 8) by adding the splitting regime at temperatures above the gap: the fluid-2D-solid phase (which is obtained by a reorientation of cholesterol as introduced above, the fluid lipid layer, and the solid cholesterol layer) extends the fluid-fluid miscibility gap in the DMPC:cholesterol phase diagram (Fig. 1) to higher temperatures. Figure 8 is characteristic of an attractive short-range interaction potential [39] acting between the lipid and the cholesterol. Note that the dominant

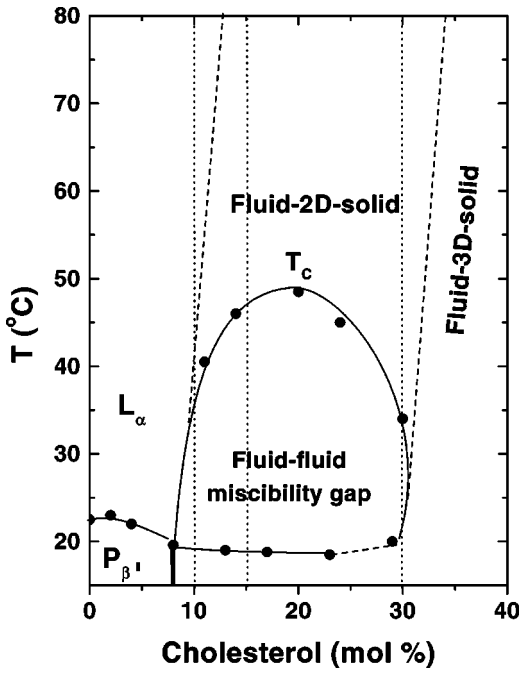

FIG. 8. Extended phase diagram for DMPC:cholesterol: The phase separating regime—denoted fluid-2D-solid, referring to the anhydrous cholesterol layer sandwiched in the lipid membrane—extends the fluid-fluid miscibility gap to higher temperatures. The dashed lines are only suggested phase boundaries as we here have not tested the phase boundaries, including the high temperature boundary of the fluid-2D solid phase. At higher cholesterol concentrations 3D sterol crystals coexist with fluid crystalline DMPC. We denote the high cholesterol part of the phase diagram as the fluid-3D-solid regime. The maximum solubility of cholesterol in phosphatidylcholines under equilibrium conditions is about $x_c = 0.66$ [38]. The dotted lines again indicate the temperature scans run, and used, in this work.

interactions in the hydrophobic membrane core (the van der Waals and steric interactions) as well as the hydration force are indeed of short range. The occurrence of the fluid-2D-solid phase is largely due to the confined bilayer geometry. The bilayer itself has its origin in the amphiphile character of lipid molecules.

In our analogous experiments with dipalmitoylphosphatidylcholine and cholesterol, and with DMPC and androsten in the same concentration range, a similar decrease in intensity but no phase separation was detected (unpublished data from this collaboration). Considering a vertical movement [34] of the sterols these findings can be understood, because DPPC has two methylene groups more per chain than DMPC. This length appears to be too long to allow the cholesterol to move to the center of the bilayer. Androsten, which resembles cholesterol shortened by the extra aliphatic tail [16], is too short compared to the $C14$ chains of DMPC, so that it does not move to the center of the bilayer to form the 2D-sterol crystal. These two cases suggest that the relative length of the sterol chain to the lipid chain is a parameter which determines the structural polymorphism of the binary lipid-:sterol mixtures. The single bilayer prevails as long as the (hydrophobic) length ratio between lipid chains and sterol

[16] is above a characteristic number at which we observe the phase separation.

C. Energy vs entropy

In view of the theory of binary liquids [40] the transition from the fluid-fluid miscibility gap to the phase-separated regime, when raising the temperature (Fig. 1), as well as the growth of domains in the gap, can be understood as a loss of entropy. Also, a transition from the (expected) miscible part of the phase diagram at higher temperatures into the phase-separated regime is accompanied by an entropy loss. This would mean that the fluid-fluid miscibility gap represents a low temperature region of entropy dominance in the phase diagram of the DMPC:cholesterol mixture. Similarly, the fluid-2D-solid phase represents a higher temperature ''ordered'' phase.

V. CONCLUSIONS

The interactions intrinsic to the fluid dimyristoylphosphatidylcholine:cholesterol system in excess water permit the observation of a phase separation taking place in a lipid system. To explain the existence of two ordered phases for cholesterol concentrations $x_c \geqslant 0.15$ at temperatures above the fluid-fluid miscibility gap (Figs. 2 and 3), we introduce a model that allows for reorientation of cholesterol within the bilayer (Fig. 7). The demixing of cholesterol in DMPC (leading to a phase separation) can be understood as a movement of the hydrophobic cholesterol toward the hydrophobic core of the bilayer with increasing temperature. This process eventually leads (with increasing temperature) to a macroscopic phase separation yielding two phases within the bilayer, which differ in the orientation of the cholesterol long axis with respect to the hydrophilic-hydrophobic interface. Our model is depicted in Fig. 7, and by a phase diagram in Fig. 8. We suggest NMR or neutron diffraction experiments to crucially test our model, as such studies have, to our knowledge, not been performed in the splitting regime.

The coexistence of two lamellar phases—the phase-separated regime—in a temperature range above the miscibility gap, i.e., in the miscible part of current phase diagrams [1,4], looks contradictory at first glance. Then one recalls that the conventional phase diagram leans on the equilibrium thermodynamics of a binary fluid. However, the lipid:cholesterol mixture studied is not an ideal binary fluid.

The bilayers of different thickness responsible for the two lamellar phases [Fig. 3(a)] may be considered a stable morphological intermediate between lamellar and nonlamellar phases, that are supposedly involved in processes such as cell fusion; cholesterol has been reported to promote the formation of nonlamellar phases in polyunsaturated PC's [41]. Also, a stable phase separation in a binary mixture has been observed to be involved in vesicle fusion [11,42]. By reducing the steric repulsion, when moving into the phase-separated regime, the DMPC:cholesterol system can avoid a transition to inverted nonlamellar phases. Besides sterols, other largely hydrophobic additives, e.g. diacylglycerols or fatty acids, should likewise be able to move vertically in the membrane; the more flexible of them are known to induce nonlamellar phases [43]. In the nonlamellar phases, the lipid:fatty acid mixtures indeed show a partial phase separation. The fatty acid appears to predominantly fill the topological interstices of the inverted hexagonal phase [44,45]. Characteristics such as immiscibility and stoichiometry also play a prominent role in these mixtures. Also, small peptides such as cyclosporin A [46] may be suitable candidates as nonlamellar phase inducers.

Finally, our temperature jump experiments indicate that the degree of miscibility does not depend on the degree of nonequilibrium (Fig. 6), i.e., the domain structure cannot be governed exclusively by the interactions intrinsic to DMPC and cholesterol molecules. The higher degree of amphiphilicity, and thus the higher preference for water of the DMPC in the DMPC:cholesterol system, is suggested here to stabilize the two coexisting lamellar phases above the miscibility gap. It can be expected that other molecules with a preference to interact with water, e.g., certain proteins, are also able to force the cholesterol toward the bilayer core. The extended phase diagram (cf. Fig. 8) mirrors this result. We note that the system studied, DMPC:cholesterol, appears to be a realization of the mechanism of a metastable critical point-assisted nucleation [39]. Our system indeed supports the general suggestion that this mechanism occurs both in the bulk—the fluid-3D-solid regime—and in quasi-two-dimensional systems, such as membranes.

ACKNOWLEDGMENTS

L. F. and G. R. thank NATO for Grant No. CRG 970225. The support of the German BMBF to F.R. through Grant No. 03-SA4TU2-5 is gratefully acknowledged.

[1] E. Sackmann, in *Structure and Dynamics of Membranes*, edited by R. Lipowsky and E. Sackmann (North-Holland, Amsterdam, 1995).

[2] *Cholesterol in Membrane Models*, edited by L. Finegold (CRC, Boca Raton, FL, 1993).

[3] J. H. Ipsen, O. G. Mouritsen, and M. J. Zuckermann, Biophys. J. **56**, 661 (1989).

[4] R. N. McElhaney and T. P. W. McMullen, Biochim. Biophys. Acta **1234**, 90 (1995).

[5] R. Bittman, *Subcellular Chemistry* (Plenum, New York, 1997).

[6] E. Strauss, Science **280**, 1528 (1998).

[7] T. M. Bayerl and E. Sackmann, in *Cholesterol in Membrane Models* (Ref. [2]).

[8] P. F. F. Almeida, W. L. C. Vaz, and T. E. Thomson, Biochemistry **31**, 6739 (1992).

[9] F. Richter, L. Finegold, and G. Rapp, Phys. Rev. E **59**, 3483 (1999).

[10] P. A. Reis and H. M. McConnell, Proc. Natl. Acad. Sci. USA **86**, 6445 (1989); C. L. Hirshfeld and M. Seul, J. Phys. (France) **51**, 1537 (1992).

[11] E. Sackmann, Can. J. Phys. **68**, 991 (1990).
[12] M. P. Marsan *et al.*, Biophys. J. **76**, 351 (1999).
[13] O. G. Mouritsen, Chem. Phys. Lipids **57**, 179 (1991).
[14] M. J. Zuckermann, J. H. Ipsen, and O. G. Mouritsen, in *Cholesterol in Membrane Models* (Ref. [2]).
[15] J. R. Silvius, D. del Giudice, and M. Lafleur, Biochemistry **35**, 15 198 (1996).
[16] L. Finegold and M. A. Singer, in *Cholesterol in Membrane Models* (Ref. [2]).
[17] G. Rapp, A. Gabriel, M. Dosière, and M. H. J. Koch, Nucl. Instrum. Methods Phys. Res. A **357**, 178 (1995).
[18] G. Rapp and R. S. Goody, J. Appl. Crystallogr. **24**, 857 (1991).
[19] T. C. Huang, H. Toraya, T. N. Blanton, and Y. Wu, J. Appl. Crystallogr. **26**, 810 (1993).
[20] A. Guinier, *Principles of X-ray Diffraction* (Freeman, San Francisco, 1963), Chap. 9.
[21] R. Zhang *et al.*, Phys. Rev. Lett. **74**, 2832 (1995).
[22] J. Lemmich *et al.*, Phys. Rev. E **53**, 5169 (1996).
[23] R. Zhang *et al.*, Biophys. J. **70**, 349 (1996).
[24] R. Zhang, R. M. Suter, and J. F. Nagle, Phys. Rev. E **50**, 5047 (1994).
[25] D. Marsh, A. Watts, and P. F. Knowles, Biochemistry **15**, 3570 (1976).
[26] S. Subramaniam and H. M. McConnell, J. Phys. Chem. **91**, 1715 (1991).
[27] J. Lemmich *et al.*, Eur. Biophys. J. **25**, 293 (1997).
[28] A. M. Petrascu, M. H. J. Koch, and A. Gabriel, J. Macromol. Sci., Phys. **37**, 463 (1998).
[29] M. Rappolt *et al.*, Eur. Biophys. J. **29**, 125 (2000).
[30] J. S. Langer, Ann. Phys. (N.Y.) **65**, 53 (1971).
[31] I. M. Lifshitz and V. Slyozov, J. Phys. Chem. Solids **19**, 35 (1961).
[32] L. K. Nielsen *et al.*, J. Phys.: Condens. Matter **12**, A309 (2000).
[33] S. Halstenberg *et al.*, Biophys. J. **75**, 264 (1998).
[34] C. Gliss *et al.*, Biophys. J. **77**, 331 (1999).
[35] M. Pasenkiewicz-Gierula *et al.*, Biophys. J. **78**, 1376 (2000).
[36] H. S. Shieh, L. G. Hoard, and C. E. Nordman, Nature (London) **267**, 287 (1977); Acta Crystallogr., Sect. B: Struct. Crystallogr. Cryst. Chem. **37**, 1538 (1981).
[37] W. Knoll, G. Schmidt, and E. Sackmann, J. Chem. Phys. **79**, 3439 (1983).
[38] J. Huang, J. T. Buboltz, and G. W. Feigenson, Biochim. Biophys. Acta **1417**, 89 (1999); J. Huang and G. W. Feigenson, Biophys. J. **76**, 2142 (1999).
[39] P. R. ten Wolde and D. Frenkel, Science **277**, 1975 (1997).
[40] D. J. Adams and I. R. McDonald, J. Chem. Phys. **63**, 1900 (1975); R. P. Sear, *ibid.* **111**, 4800 (1999).
[41] C. J. Dekker *et al.*, Chem. Phys. Lipids **33**, 93 (1983).
[42] R. Lipowsky, J. Phys. II **2**, 1825 (1992).
[43] R. Koynova, B. Tenchov, and G. Rapp, Chem. Phys. Lipids **88**, 45 (1997).
[44] G. L. Kirk and S. M. Gruner, J. Phys. **46**, 761 (1985); D. P. Siegel, J. P. Banschbach, and P. L. Yeagle, Biochemistry **28**, 5010 (1989).
[45] Z. Chen and R. P. Rand, Biophys. J. **74**, 944 (1998).
[46] T. Söderlund, J. Y. A. Lehtonen, and P. K. J. Kinnunen, Mol. Pharmacol. **55**, 32 (1998).